Cronfa - Swansea University Open Access Repository

_____

This is an author produced version of a paper published in:
Biomedical Physics & Engineering Express

_____

Cronfa URL for this paper:
http://cronfa.swan.ac.uk/Record/cronfa40283

_____

Paper:

Reynard, D., Hugtenburg, R., Estève, F. & Adam, J. (2018). Towards in vivo dosimetry for contrast enhanced synchrotron stereotactic radiation therapy based on iodine x-ray spectroscopy. _Biomedical Physics & Engineering Express, 4_(4), 045015
http://dx.doi.org/10.1088/2057-1976/aac2f4

_____

ACCEPTED MANUSCRIPT

Towards in vivo Dosimetry for Contrast Enhanced Synchrotron Stereotactic Radiation Therapy based on iodine X-ray Spectroscopy

Towards *In Vivo* Dosimetry for Contrast Enhanced Synchrotron Stereotactic Radiation Therapy based on iodine X-ray Spectroscopy

Dimitri Reynard[1,3], **Richard Hugtenburg**[3], **François Estève**[2], **Jean-François Adam**[2]

[1]Université Grenoble Alpes, 15 rue des Universités, St Martin D'Heres, 38400, France
[2]E.A. Rayonnement Synchrotron et Recherche Médicale, Université Grenoble Alpes, Grenoble, France
[3]Swansea University, Singleton Park Campus, Sketty, Swansea SA2 8PP, UK

E-mail: `jean_francois.adam@esrf.fr`

Abstract. The first trial applications of Contrast-Enhanced Synchrotron Stereotactic Radiation Therapy (SSRT) is underway since June 2012 at the European Synchrotron Radiation Facility (ESRF) in Grenoble (France). The phase I-II clinical trial is designed to test the feasibility and safety of SSRT through a dose escalation protocol. Contrast enhanced radiotherapy achieves localized dose enhancement due to higher photoelectric effect rate in the target. This increase is obtained through the preferential uptake of high-Z media (iodine) in the tumoral area combined with irradiations with medium energy synchrotron X-rays. *In vivo* dosimetry (i.e. experimental dosimetry in real time during the treatment) would be a serious added value to the project, in terms of online dose monitoring and quality control. It is challenging to perform *in vivo* dosimetry with the currently available conventional clinical techniques. In this work we investigated a method using X-ray fluorescence detection to derive the iodine concentration contained in a tumor during the treatment of a patient, as a first step towards *in vivo* dosimetry. A mean iodine concentration of 0.33 ± 0.22 mg/ml has been retrieved in the tumor of the patient compared to 2 mg/ml expected would correspond to 3% local dose enhancement in the tumor. Further work will be performed to improve the attenuation correction method. The expected amount of iodine should be 2 mg/ml in the tumor (20% dose enhancement). This method is suitable to detect iodine in the target but has some problem in quantifying the real amount of iodine present during the irradiation.

This study takes place within the scope of phase I/II clinical trials of Stereotactic Synchrotron Radiation Therapy (SSRT). The trial is designed to prove the feasability and safety of SSRT through a dose escalation protocol. The patients who benefits from this modality suffer from brain metastasis of medium to small volume.

SSRT consists in loading a tumor with an iodinated contrast agent (CA) through intraveneous injections. The CA selectively leaches into the tumor because of the localised blood brain barrier (BBB) permeabilisation [1]. The impaired BBB and hence

2

iodine biodistribution is directly related to the tumor presence. Moreover the iodine is located in the interstitial space and in the vessels so the dose will be delivered to the target cells and neovasculature, under the assumption of an homogeneous emission of the secondary particle. [2]. The combination of CA and a stereotactic irradiation with mono-energetic kilovoltage X-rays produces a gradient in the absorption cross-section leading to an increased dose deposition [3]. A differential effect is produced between the tumor and the healthy brain depending on the iodine uptake, leading to a difference in the photon interaction mechanisms. The photoelectrons produced in the target volume deposit their energy over a sub-millimetric distance in the vicinity of heavy atoms, whereas Compton scattering predominates in the surrounding healthy tissues. As a consequence, the dose deposition upstream and downstream the tumor is further reduced while the dose in the tumoral tissue is reinforced. This differential effect is a substantial added value to the high energy treatments performed nowadays. Robar et al studied the use of iodine as a radiosensitizer in conventional SRT (energy beam ranging from 2 MV to 18 MV) and reported a dose enhancement factor (DEF) for iodine concentration around 3 mg/ml of iodine of less than 1.6 % [4]. On the other hand Edouard et al reported a DEF of 10% per mg/ml of iodine during the SSRT treatment [5]. At high energy, the DEF is then negligible, hence the necessity of using a low-medium energy x-ray source. In order to achieve a satisfying DEF a synchrotron source is not mandatory, only the photon energy matters. A first clinical trial performed in the 90's [6] used a modified X-ray tube and presented a total treatment time of 45 minutes (3x15 mins with cooling periods in between) because of the need of cooling down the x-ray tube. However, a synchrotron offers significant advantages compared to a conventional x-ray tube, in offering tunable monochromatic high flux x-ray beam, and a substantial reduction of the treatment time (20 mins including positioning), and the optimal energy between high DEF and low dose to the bone can be chosen. [5] The iodine injection is thus only used for the SSRT fraction of the treatment.

There is a linear relationship between the localized dose enhancement and the iodine concentration, as shown by [7]. A localized 10% increase per mg/ml is achieved in the tumor when compared to an irradiation at the same energy, without contrast agent. The treatment planning system is taking the iodine presence into account for the calculation (Monte Carlo based treatment planning system) As well as radiotherapy programs, innovative X-ray imaging techniques using the inherent properties of synchrotron radiation such as the high photon flux density, the broad energy spectrum, the natural collimation and the linear polarization are under active developement.

Fluorescence spectroscopy is commonly used to detect low contents of specific heavy atomic number elements in material science. Until now fluorescence hadn't been used to assess the iodine concentration and its resulting dose enhancement. Applying this technique to medical imaging, it becomes conceivable to track down the iodine uptake of an organ without the low sensitivity of conventional CT acquisitions [8]. The measurement of the distribution of iodine within the thyroid gland [9] has been made using Fluorescence X-ray Computed Tomography (FXCT) [10]. Later in 2005 the

3

cerebral perfusion of a living mouse has been retrieved using FXCT [11]. Nevertheless, FXCT is not appropriate for the purpose of SSRT for reasons linked to the irradiation time, and scale problems due to the brain and skull thicknesses in human. Moreover, the small detection volume in the detector makes the measurement of fluorescence X-rays a rare event due to small detection solid angle, so compromise between spatial resolution and measurement's statistical reliability has to be found.

During SSRT treatment, the irradiated iodine atoms emit characteristic X-rays (K_α line at 28.5 keV) whose amount depends directly on the iodine concentration in the tumor. The exact measurement of the tumor's CA uptake would be a serious added value in terms of on line dose monitoring and quality assurance. In any case, it should be noted that the irradiation in SSRT consists on 3 to 10 weighted beams distributed around the patient's skull, which is an other reason why FXCT as commonly used is not appropriate. The substantial thickness of tissue in human skull and the low number of beams incidence are technical rationales sufficient to investigate a simpler alternative to FXCT, in which 3D iodine average concentration can be retrieved.

Therefore the aim of this work is to examine the feasibility retrieving absolute iodine concentration in real time during the SSRT treatment as a first step towards *in vivo* dosimetry in SSRT. The feasability of fluorescence detection was examined by preliminary Monte-Carlo simulations using the code PENELOPE (Penetration and ENErgy LOss of Positrons and Electrons) involving an analytical human head phantom as the geometry used for parametric study [7]. A calibration data of iodine content was obtained from tubes filled with various concentrations of iodine and irradiated with synchrotron monochromatic low-energy X-rays. A model was then developed to relate the fluorescence rate detected to the iodine amount. Finally this model was used to determine the average iodine concentration in patients tumors during treatments. This is the first mandatory step to propose an in vivo dosimetry modality in SSRT.

1. Material and Methods

1.1. Monte-Carlo Simulation

The aim is to retrieve the signal generated by the K_α line of iodine which is at an average energy of 28.5 keV composed of $K_{\alpha1}$ (28.61 keV) and $K_{\alpha2}$ (28.32 keV) and accounts for about 85% of the lines produced after a K-shell ionisation [12], the other 15% are coming from Auger emission. At these energies the average mass attenuation coefficient of the brain tissue is around 0.3811 cm^2/g (1.331 cm^2/g for the skull,bone, ICRU-44 [13]). By considering a tumor 5 cm in depth behind a skull of 1 cm thick, we can simply calculate the amount of fluorescence that comes out from the head using the Beer-Lambert law in a given direction. It is less than 0.05% of the fluorescence generated. Moreover, the detector receives only photons emitted in a well defined solid angle which results in a further fall of the count rate due to the isotropic fluorescence emission.

The environment of the tumor (brain, skull, skin) and its size enlarges the scat-

4

Figure 1. (a) Ellipsoid phantom used for the simulation (b) Iodine fluorescence signal collected in a 3x3x1 mm^3 CZT volume
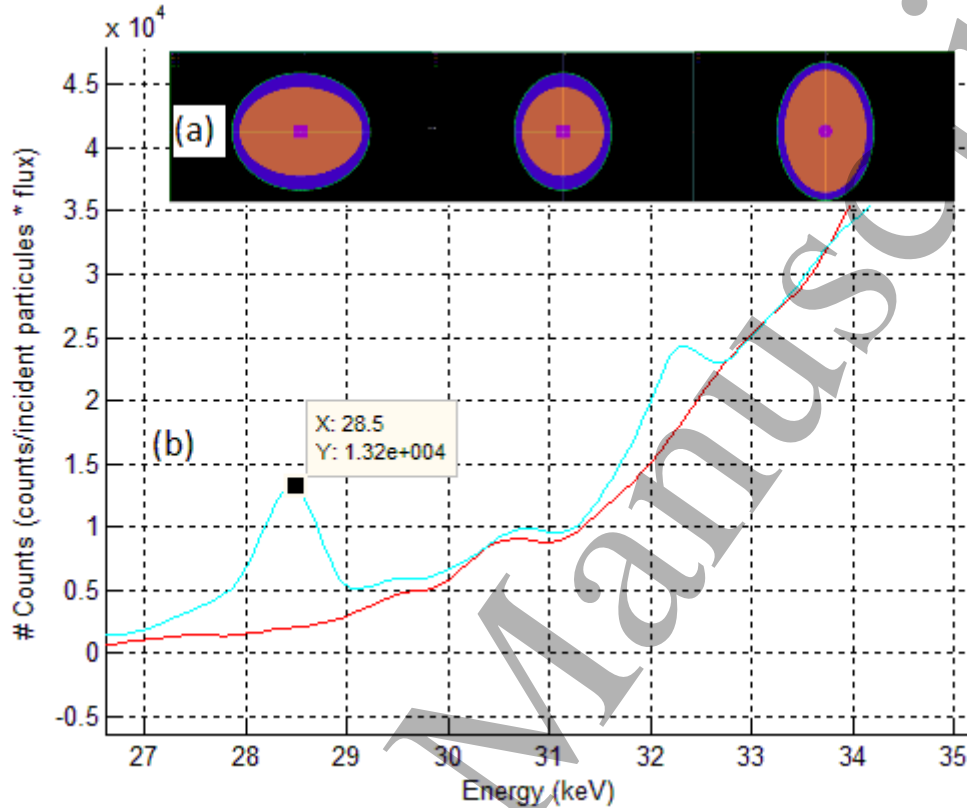
tered photon rate which could in a sense worsen the signal to noise ratio (SNR). As a consequence, the first point that is investigated is the feasability of the spectrometric measurement in SSRT by the mean of Monte-Carlo simulations. For this purpose, the Monte-Carlo code PENELOPE is used together with code PENGEOM to define geometry files (bodies).

An analytical human head phantom is used, described by Bouchet & al [14] adapted from nuclear medicine studies using the MIRD formalism. A tumor is modeled by a cylinder (2 cm height, 2 cm diameter) filled with a homogeneous mixture of brain material and iodine at various concentrations ranking from 0 to 20 mg/ml. The tumor is positionned at the center of the brain as shown in Figure 1. The materials that fill the bodies are adapted from the database of the ESTAR program of Berger [15] for the brain, skull and skin. As far as mixtures and compounds are concerned, the weighted sum method is adopted to define the material cross sections, which means that the corresponding molecular cross section is set equal to the sum of atomic cross sections weighted with the stoichiometric index of the element.

A small CdZnTe (CZT) cuboid of 3x3x1 mm³ is set as an energy deposition detector and placed according to the x-axis. Finally, the simulated beam is a 2x2 cm² square field, polarized, parallel and monochromatic at the energy of 80 keV emitting photons along the

5

Figure 2. Set up used for fluorescence measurement on patients. In case of the acquisition of the calibration curve, tubes were not placed in head phantom.
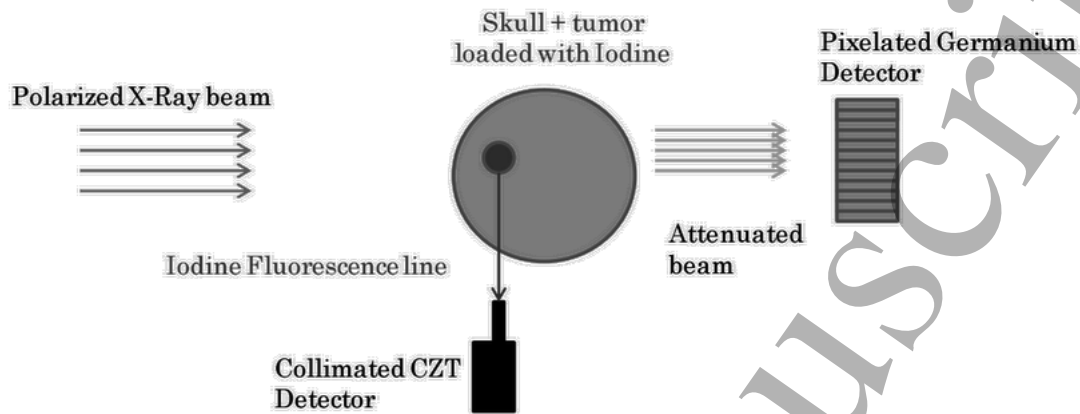
y-axis to form a 90 degrees angle with the detector. The irradiation is performed in the xy-plan and the number of photons simulated accounts for 10^9. Electron and photon cut-of are both set at 25 keV as this value is lower than the $K_{\alpha1}$ and $K_{\alpha2}$ for iodine and particles with such energy cannot produce fluorescence from the iodine K edge which is of interest here. Coefficients C1 and C2 are both set at 0 for a fully detailed simulation of the scattered radiation. The spectra obtained are then processed to simulate a real spectrum acquired with a CZT detector [16]. This numerical treatment distributes a certain amount of counts from the full energy peak at lower energy channels, and the peak is enlarged as a Gaussian distribution. In other words, the procedure considers the statistical spread in the number of charge carriers and charge collection phenomena. The MC simulations are performed to evaluate the fluorescence detection feasibility in a clinical case.

1.2. Analytical Model for Iodine Concentration Quantification

As the fluorescence rate depends on the iodine concentration, the volume irradiated, the incident flux and the irradiation time, a calibration curve is realized to characterize the iodine concentration in the tumor.

The set up used is basically an FXCT set up as described on Figure 2 with a Amptek CZT detector with a detection volume of 3x3x1 mm^3 placed at 90 degrees of the incident beam and at 155.2 cm from the isocenter. This way of positioning the fluorescence detector reduces the background from Compton scattering. This improves the detectability of the fluorescence X-rays by taking advantage of the linear polarisation of the synchroton beam [17]. A 2 millimeters pinehole is used to geometrically select the photons coming from the isocenter and to reduce the amount of scattered photons detected. Despite these collimation elements a significant aperture remains and represents a circle of 15 cm in radius at the level of the isocenter.

6

Figure 3. Irradiation geometry used in the analytical modelling of the calibration curve.
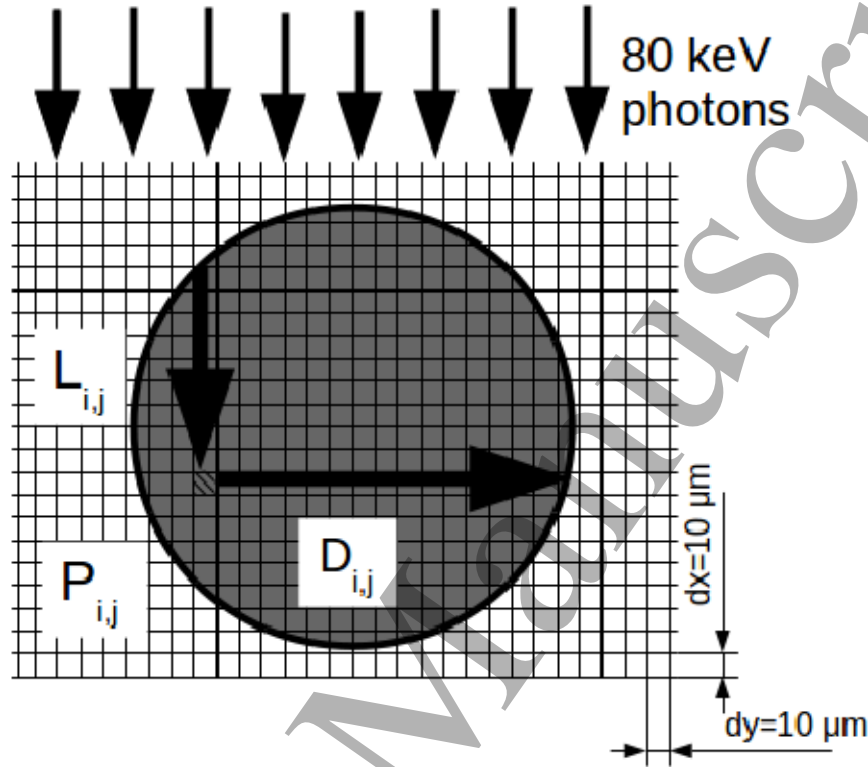
An array of solutions with concentrations varying from 0 to 20 mg/ml are prepared and placed into cylindrical plastic tubes of 3 cm in diameter and 3 cm high. Absolute iodine concentrations is derived from monochromatic computed tomography (CT) images of the tubes using the subtraction of a CT image of a tube filled with pure water [18]. The tubes are thus irradiated with a 2 mm thick beam at 80 keV using 2 irradiation modes, static and bottom to top scanning with the same irradiation time. Finally, the spectrum acquired are processed to remove the background from scattered photons using the 3 channels method [19] and to extract the fluorescence rate.

This simple experiment is also simulated using MatLab (MATLAB 9.1, The MathWorks Inc., Natick, MA, 2000). The tube is divided into pixels 10 μm x 10 μm ($dx \times dy$) as shown of Figure 3. The emitted fluorescence $f_{i,j}$ in a given pixel $P_{i,j}$ is calculated with equation 1. If we assume an equal iodine concentration $[I]$ for each pixel of the target, the amount of fluorescence delivered by a given pixel $P_{i,j}$ depends only on the amount of pixels filled with iodine that the photon flux Φ impacts before the interaction with the pixel emitter. This number multiplied by dx defines the depth $L_{i,j}$ for each pixel $P_{i,j}$ with regards to the entrance beam.

$$f_{i,j} = \tau \mu_{pe80} dx \cdot \Phi e^{-\mu_{80} \cdot L_{i,j}} \tag{1}$$

Table 1. Irradiation/Simulation parameters

Φ	$3 \cdot 10^{12} \ ph/cm^2/s$
Beam width	3 cm
Beam height	2 mm
τ	0.8
Ω	$3.18 \cdot 10^{-7}$ sr

With τ the fluorescence yield of the K_α line of iodine μ_{pe80} and μ_{80} the linear attenuation coefficient of the photoelectric effect at 80 keV for the solution in a given voxel, dx the length of the pixel and total attenuation coefficient respectively, Φ the ESRF photon fluence, $L_{i,j}$ the depth of the pixel $P_{i,j}$. Considering the distance $D_{i,j}$ of the emitted fluorescence $f_{i,j}$ in the direction of the detector inside the tube, the detected fluorescence is calculated using equation 2.

$$f_{det}(I) = \frac{\Omega}{n} \sum_{i,j} f_{i,j} e^{-\frac{\mu_{tot}([I])}{\rho} \rho \cdot D_{i,j}} \tag{2}$$

with $\frac{\mu_{tot}([I])}{\rho}$ as the total linear attenuation coefficient of the iodine mixture calculated in the diluted approximation solution using equation 3.

$$\frac{\mu_{tot}([I])}{\rho} = \left[\frac{\mu}{\rho} \right]_{H_2O} \times (1 - [I] \cdot 10^{-3}) + \left[\frac{\mu}{\rho} \right]_I \times [I] \cdot 10^{-3} \tag{3}$$

Where Ω the solid angle defined by the emitting pixel to the aperture of the detector, n is the number of pixels in the tube. Using the irradiation parameters described by Table 1. The results of the calculation are compared to the fluorescence measurement to validate the calibration curve.

1.3. Measurement during patient treatment

The experimental set up is exactly the same as in the previous part (Figure 2). The tumor of the patient is placed at the isocenter of the treatment room and the irradiation is performed using several incidences (3 to 8 for the 3 patients studied here).

In order to maximise the spare of healthy tissue, every beam is shaped by a Cerobend mask placed between the X-ray source and the patient, according to the limits of the Plan Target Volume (PTV) plus a 3 mm margin. The fluorescence spectrums are acquired for every beam incidences and processed to retrieve the iodine concentration in the tumor. Figure 4 shows a print screen of the treatment plan used in SSRT and allows the visualisation of the beam incidences.

Firstly, spectrums are filtered using a low pass filter in the Fourier space to remove the statistical noise which is expressed through fast oscillations. Both the peak stripping method and the 3 channels method are used to remove the background and return the

8

Figure 4. CT Scan extracted from the TPS. The tumor is irradiated with 8 weighted beams (bottom right hand corner). The material segmentation (bottom left hand corner) shows the ring shaped iodine uptake at the isocenter height.
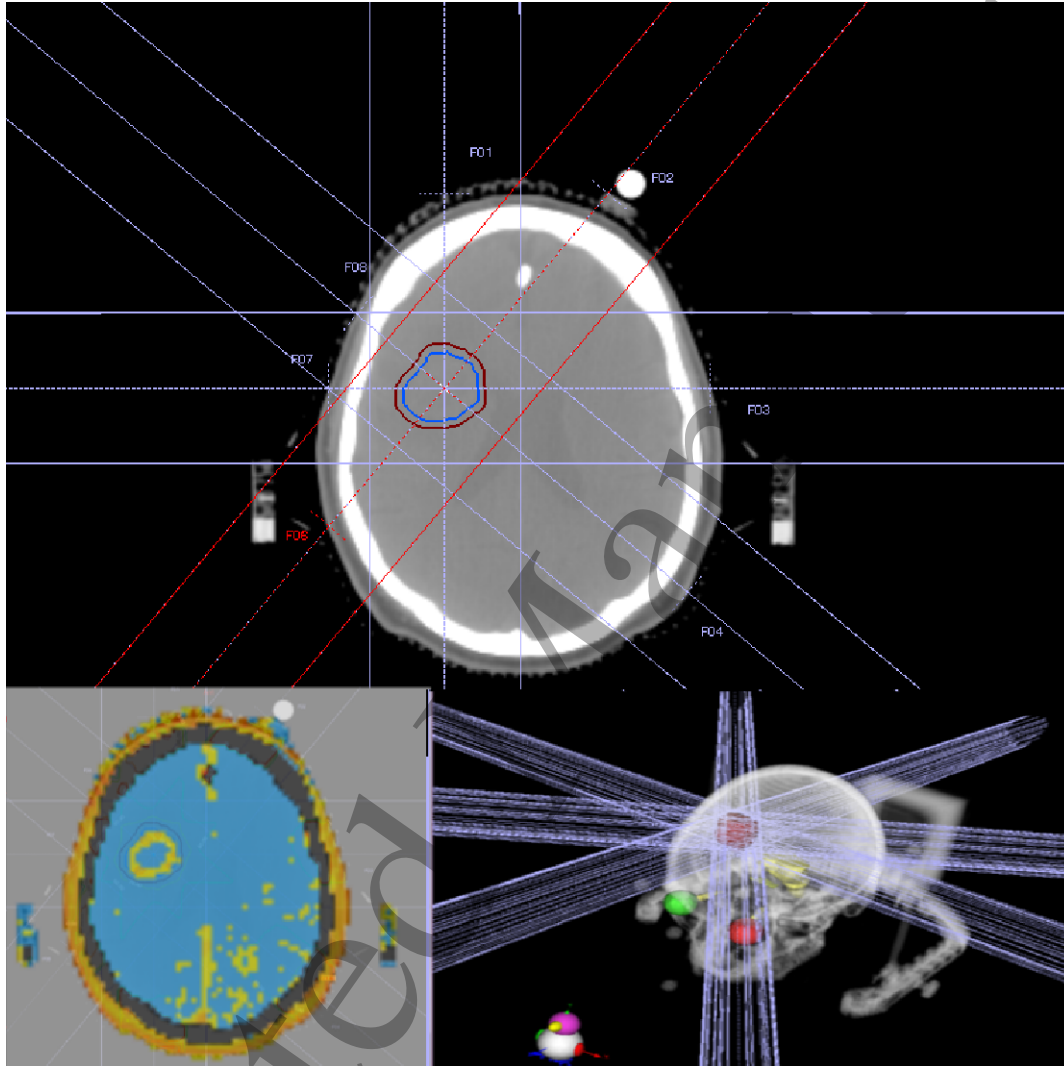
same results. Peak stripping method is a way of spectrum calculation that detects peaks and iteratively merges them to the background line [19]. As for the 3 channels method, it geometrically adjusts a trapezium under the peak and removes it.

For the spectrum calculation only the 3 channels method is used because this technique is the fastest.

In the general case, when the fluorescence rate is retrieved for each beam incidence, a normalisation procedure sould be applied. The idea is that the total irradiated volume is set by the Cerobend masks which shapes come directly from the TPS and is not depending on the irradiation incidence. Therefore the iodinated irradiated volume remains the same during the whole treatment. Retrieving the iodine concentration in the tumor would require the normalization of the fluorescence rate to the same irradiation conditions as the tubes in order to compare directly the fluorescence rate

9

in both cases. Such normalization should account for the irradiation time, the photon flux which decreases with time and tissue attenuation. But in SSRT one can benefit from the fact that each of the irradiation port delivers the same dose to the isocenter ($\frac{1}{8}$ of $7Gy$). One key aspect that is investigated is how the measured fluorescence varies with the dose to the medium. In the case where the dependence is proportional, the normalization to the incoming fluence becomes pointless and the only remaining step between fluorescence measurement and iodine concentration retrieval is tissue attenuation correction for 28.5 keV photons (Iodine's K_{alpha} line). For this purpose, a serie of MC simulations involving tubes 3 cm in diameter 3cm high filled with 5mg/ml of iodinated solution and 1 cm thick slabs of brain material is used. The brain slabs are positioned between the 80keV photon source and the tube. The brain thickness ranges from 1 cm to 4 cm. In the mean time the same experiment is realized with a tube filled with 5mg/ml of iodinated solution and brain slabs from the CIRS (CIRS, Norfolk, VA ,USA), radiosurgery phantom MODEl605.

The beam used for the imaging procedure is the same used for the treatment which is a monoenergetic 80 keV beam. At the ESRF the tomography reconstruction algorithm generates CT scans where pixel values are the linear attenuation coefficient at the scanning energy.

Therefore, tissue attenuation correction for 28.5 keV photons is computed from a patient specific CT scan realized between the iodine injection and the patient irradiation. The resolution of the CT scan is 841x841 with a pixel size of 336×336 μm^2 The extrapolation of mass attenuation coefficient obtained on the CT image tothe value required for 28.5 keV photons is calculated using the method described by Schneider & al [20]. In this method the Hounsfield units (in our case the grey values of the image) at a given energy of each material are sorted. Any in between Hounsfield unit present in the image is then described as a mixture of the two elements matching two closest material Hounsfield unit values. The mass attenuation coefficient at 28.5 keV from the NIST database for each material is finally used to extrapolate the CT image at 28.5 keV.

For the purpose of this work 3 regions are defined. The first one is a mixture of brain tissue and iodine. [8] has stated that a small amount of iodine remains in the brain tumoral tissue after the injection so this segmentation is applied for Hounsfield units close to the tumoral tissue. For regions close to the bone, materials are described as a mixture of brain and spongy bone. The skull being a sequence of spongy bone and cortical bone, any Hounsfield unit around the spongy bone value will be treated as a mixture of spongy bone and cortical bone. The last region is treated as cortical bone only. Figure 5 shows a profile from the 80 keV CT scan. The values of the linear attenuation coefficient for each material is extracted from the NIST database. The mixtures are calculated as a weighted sum of two materials. Considering μ_1 and μ_2 the linear attenuation coefficient at 80 keV from the NIST database of two materials composing the mixture and α and β the mass fractions. Any $\mu_1 < \mu_{ib} < \mu_2$ in between

10

Figure 5. Profile from the 80 keV CT scan. Distance 0 is at the isocenter and the profile crosses the brain and the skull.
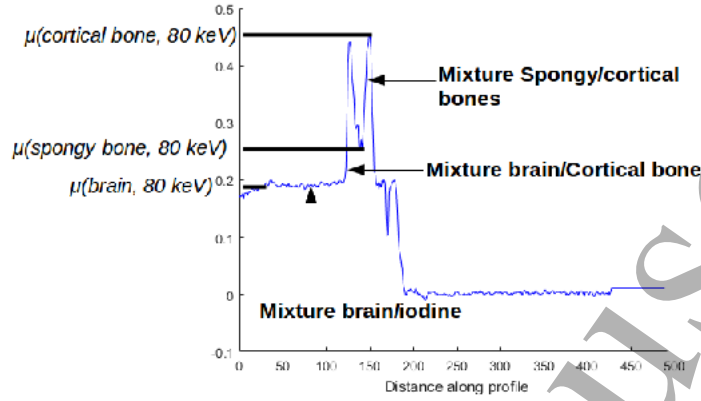
(ib) linear attenuation coefficient in the image be written as:

$$\begin{cases} \mu_{ib} &=& \alpha\mu_1 + \beta\mu_2 \\ 1 &=& \alpha + \beta \end{cases} \tag{4}$$

Solving the equation leads to:

$$\begin{cases} \beta &=& \frac{\mu_{ib} - \mu_1}{\mu_2 - \mu_1} \\ \alpha &=& 1 - \beta \end{cases} \tag{5}$$

The coefficients α and β are then used for each pixels to attribute an extrapolated value of the linear attenuation coefficient at 28.5 keV $\mu_{e,28.5keV}$ as given by equation 6 where are the linear attenuation coefficient of the materials at 28.5 keV from the NIST database.

$$\mu_{e,28.5keV} = \alpha\mu_{1,28.5} + \beta\mu_{2,28.5} \tag{6}$$

The linear attenuation coefficient used at 28.5 keV are $\mu_{tot} - \mu_{Rayleigh}$. As a matter of fact, including Rayleigh scattering in the linear attenuation coefficient means that a photon that interact through Rayleigh mechanism will not be detected. The 15 cm in radius aperture at the level of the isocenter makes Rayleigh photons detectable by the CZT detector. The tissue attenuation is finally corrected using the extrapolated 28.5 keV CT scan. For each irradiation port the attenuation coefficient is calculated as the mean coefficient in a cone from the isocenter and limited by the size of the active volume area of the CZT detector which represents an average over 10 lines.

2. Results

Monte-Carlo Simulation

The Monte-Carlo simulations provides results that confirm the feasability of fluorescence

11

detection in the case of a centered tumor. The mean concentration of iodine in the tumor volume is expected to be around 1.95±0.12 mg/ml as measured on 12 patients by Obeid & al [8]. For the simulation, a concentration of 5 mg/ml is used and leads to a SNR of 5.28 as shown in Figure 1. It is reasonably assumed that we can detect the iodine concentration in real patient. Building a calibration curve from the Monte-Carlo simulation is unrealistic because of the low statistics in the small detection volume (3x3x1 mm^3). As a consequence these simulations show that the detection of iodine on patients is feasible.

Calibration Curve

Results of the calibration are shown on Figure 6 for an irradiated volume of 1.14 cm^3 and a 1 second irradiation time. The model described in section 2.2 and the experimental data agree within the error bars for concentrations ranking from 0 to 20 mg/ml.

The calibration curve is bended which is due to the fact that the water absorbs less the photons than the iodine at a given energy. In the case of an equal absorption between the matrix and the analite the fluorescence would have a linear dependance with the analite concentration [19]. The simulated curve is slightly lower than the measured one as it comes from a calculation that only accounts for the primary interactions. Scattered radiation who's influence depends on the photon spectrum and irradiation geometry is not modelled here as its accurate quantification is not accessible analytically. The mean difference between the simulated and measured fluorescence is 15% which might correspond to the influence of the fluorescence emitted after interactions of scattered radiation in the tube. This simulation also allows the visualisation of the relative fluorescence intensity of each pixel and their contribution to the signal (Figure 7). It should be noticed that the major part of the signal comes from pixels at the edge of the tube in the direction of the detector and not from the isocenter. This is due to the attenuation of the 80 keV photons inside the tube on one hand and self absorption of 28.5 keV photons within the medium combined with the irradiation geometry on the other hand.

Measurement during patient treatment

Each spectrum acquired for each irradiation incidence is shaped like the spectrum provided by Figure 8 which is the first one ever recorded in SSRT. The intensity of the K_α line depends on the irradiation time and both the distances between the isocenter and the beam entrance point (x_1) and the isocenter to the exit point (x_2).

The red curve on Figure 8 is the result of the numerical process to remove the scattered radiation background. The correct fluorescence rate is extracted by fitting the peak with a 2 Gaussians function. The 2 Gaussians function is more appropriate to describe a photoelectric peak from a CZT detector because of its asymmetry due to incomplete

12

Figure 6. Calibration curve obtained from irradiated tubes and calculated from the model.
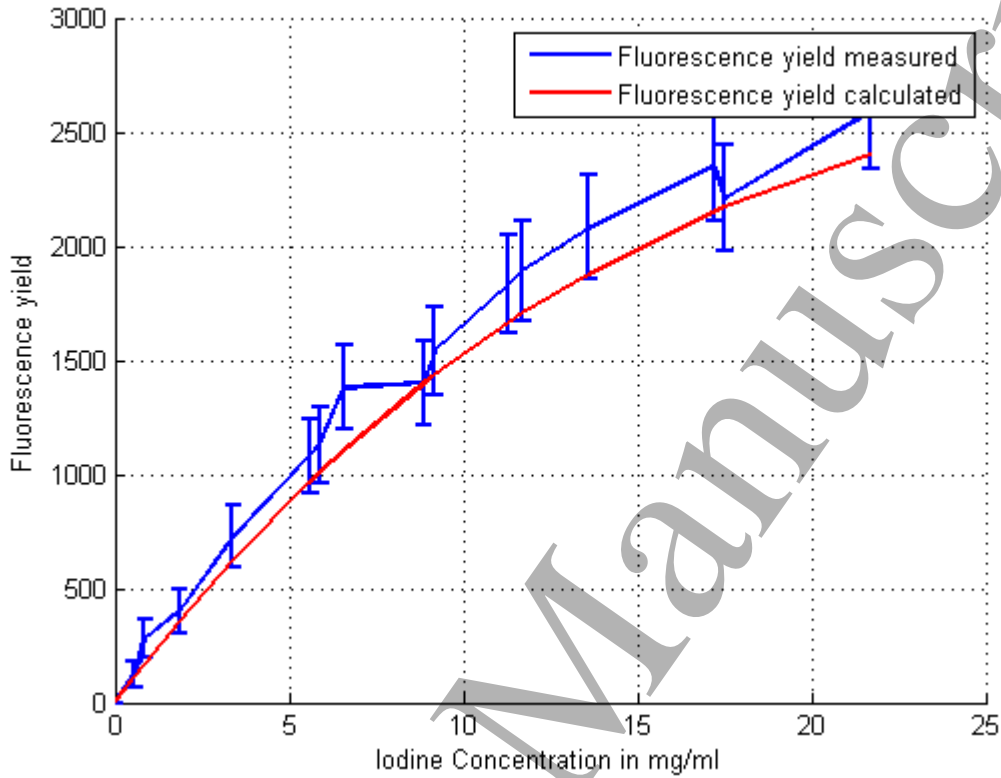
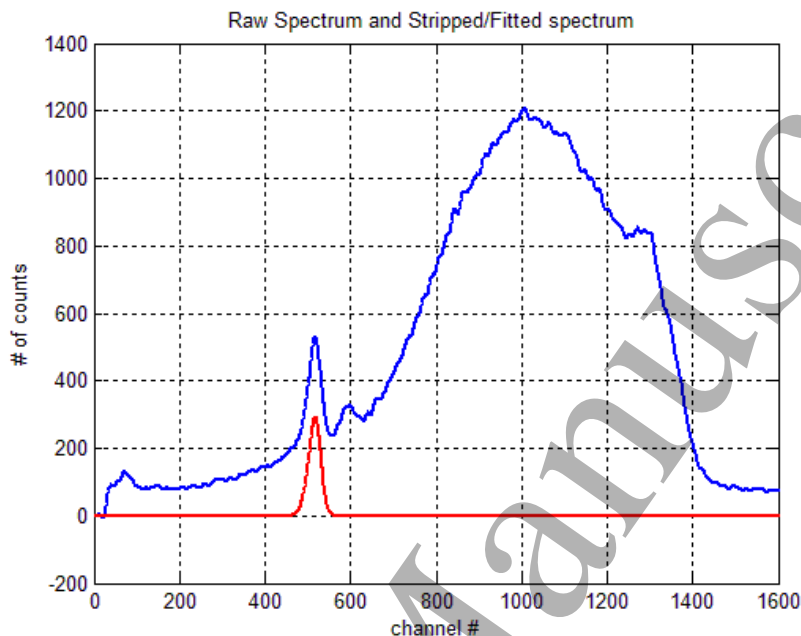**Figure 7.** (a) Relative fluorescence isotropic emission intensity in the numerical tube.(b) Relative contribution of each pixel to the measured signal.

13
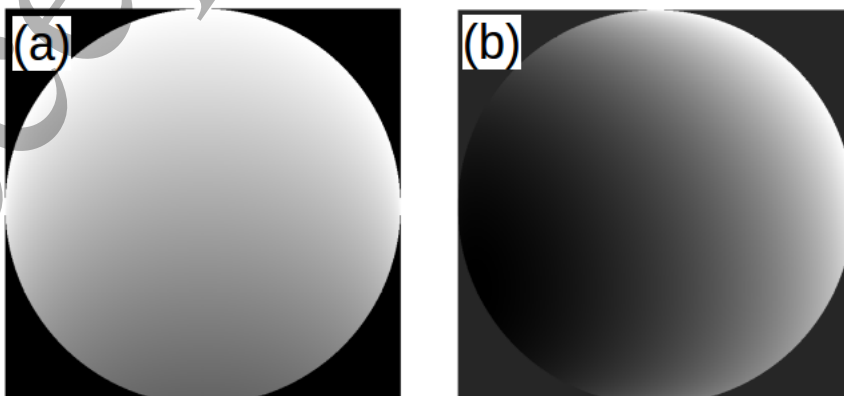
Figure 8. Spectrum detected for one irradiation incidence versus channel number. The blue line is the raw spectrum and the red line is the iodine K_α line obtained with background removal.

charge collection. The content of every channel is then summed to obtain for each irradiation incidence the detected fluorescence rate.

In order to compare the fluorescence rate to the calibration curve, a normalisation procedure has to be applied. In SSRT, each irradiation incidence deliver the same dose to the isocenter. The results of the MC study about the assumption that the fluorescence rate detected is proportional to the dose at the isocenter are shown on Figure 9. The dose and the number of counts are normalised to the maximum measured for tubes filled with 5mg/ml of iodine. The measured fluorescence and the dose calculated for tubes filled with 5mg/ml follow the same trend as the brain thickness increases, i.e. the detected fluorescence rate is proportional to the dose to the isocenter. In addition, when normalising to the dose to water, the increase in dose deposition in a 5mg/ml tude is around 50 percents which corresponds to values found in the litterature (10% increased dose per mg/ml iodine) [8].

Thanks to this calculation, the normalisation procedure becomes easier, irradiation parameters independent, but depends only on the patient geometry. The next step is then to numerically remove the tissue around the tumor by exploiting the CT image acquired with a 80keV monochromatic beam for centering the patient, and extrapolate the mass attenuation coefficient to their value at 28.5 keV. The first attempt is realized on tubes filled with 5mg/ml of iodine and the results are shown on the following table: In this case of very simple geometry, the extrapolation of the Hounsfield units from a 80 keV CT scan to 28.5 keV allows retrieving the expected fluorescence rate. The brain thickness removal produces fluorescence values in agreement with the data acquired on

14

Table 2. Fluorescence normalized to the machine current for a bare tube and corrected for brain attenuation using extrapolation method.

Irradiation conditions	Raw data /mA/s	Corrected data
Bare Tube	$52 \pm 1.5\%$	$52 \pm 1.5\%$
Tube + 1cm brain	$37.53 \pm 1.8\%$	$53.53 \pm 1.8\%$
Tube + 2cm brain	$25.53 \pm 2\%$	$51.60 \pm 3\%$
Tube + 3cm brain	$18.01 \pm 2\%$	$53.80 \pm 3\%$
Tube + 2cm brain	$13.72 \pm 2\%$	$51.85 \pm 3\%$

Figure 9. Comparison between the dose to the isocenter of the tube calculated with MC (solid line) in a 5 mg/ml iodine solution and the detected fluorescence rate (dashed line). The doted line is the dose to water.
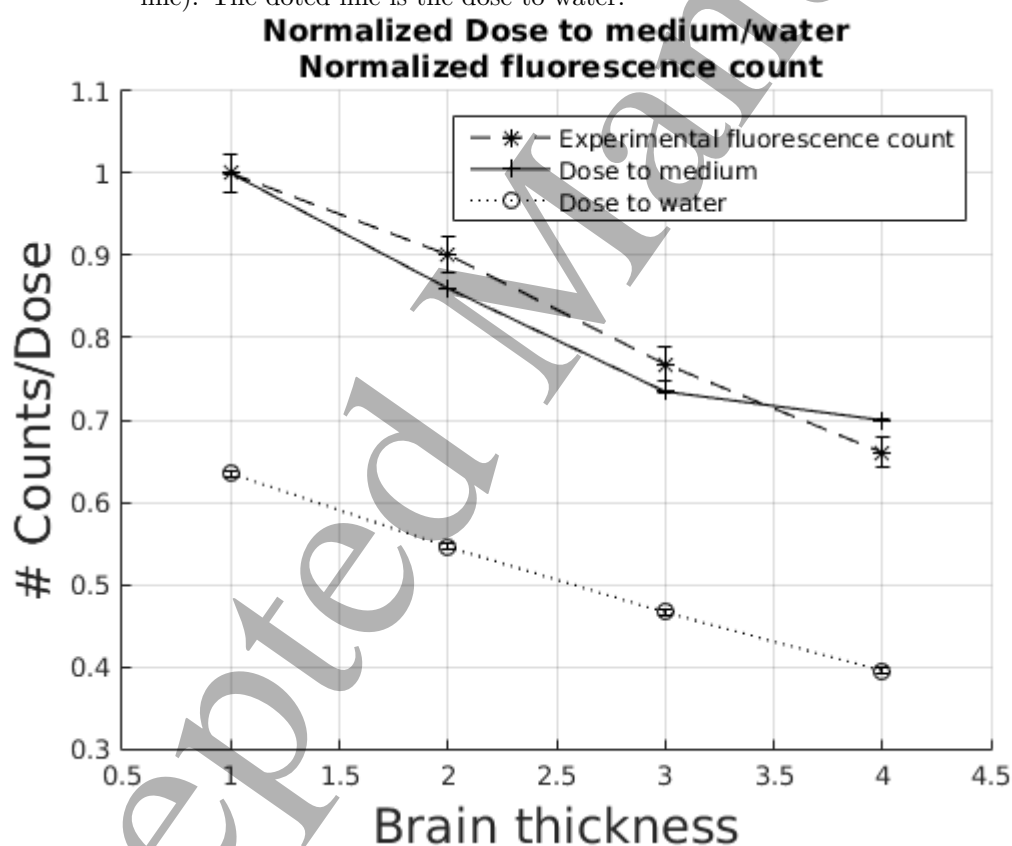
the bare tube within the error bars. Finally, the attenuation coefficient extrapolation is tested on a CT scan from a real patient, performed after the irradiation. As described in section 2.3 (Figure 4), the 80 keV CT scan is extrapolated to 28.5 keV to obtain a map of linear attenuation coefficient at this energy. The tissue thickness is then removed by acquiring pixels values on the lines from the isocenter to the detector and 10 other adjacent lines which are representative of the aperture of the detector. Figure 10 displays the corrected fluorescence rate versus the irradiation incidence. The procedure is supposed to produce the same number of counts for each irradiation port, but as shown

15

on Figure 10, the difference between the calculated fluorescence for the incidence ports can be up to a factor of 10.The additional source of uncertainties can be the detection noise, the error made using the 3 channel method and the standard deviation over the 10 lines in the CT scan and varies between 4% and 15%.

Figure 10. Fluorescence rate retrieved for each irradiation incidence.
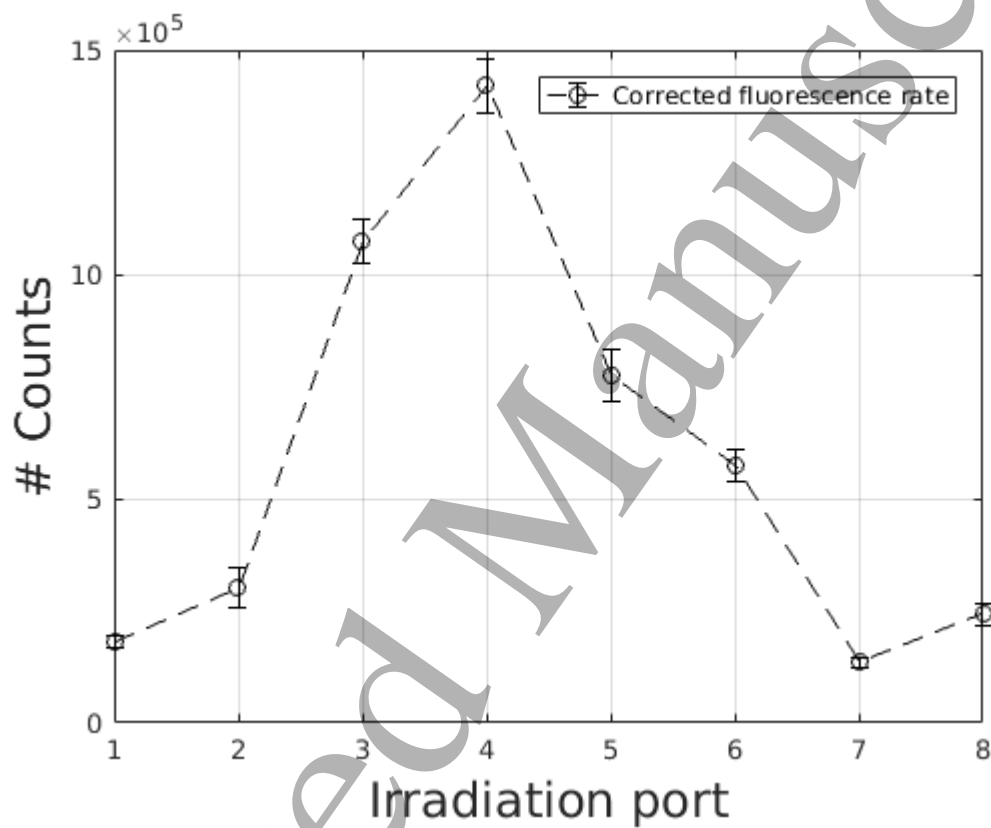
Table 3. Caption to table

Irradiation port	[I]mg/ml	Δ[I] mg/ml
1	0.102	$\pm$ 0.008
2	0.170	$\pm$ 0.025
3	0.605	$\pm$ 0.028
4	0.801	$\pm$ 0.034
5	0.430	$\pm$ 0.033
6	0.322	$\pm$ 0.019
7	0.073	$\pm$ 0.007
8	0.138	$\pm$ 0.013

16

3. Discussion

The results of the MC combined with the analytical study highlight the fact that the iodine fluorescence detection using a CZT detector is achievable. Previous studies [8] found a mean iodine uptake for 5 patients of 1.54 ± 0.19 for one protocol and 1.94 ± 0.12 for an other. But in this case, the iodine uptake is not homogeneous and is ring shaped around what appears to be a necrotic core (Figure 4). The signal coming from the edge of the tumor may be averaged because the numerical procedure assumes an emission from the isocenter and finally lowers the iodine concentration retrieval. Moreover, the CT scan being acquired after the irradiation causes the iodine to be partially washed out of the tumor.

The patient specific procedure based on the CT scan can be quantify using the linear attenuation coefficient at 28.5 keV of brain and two types of bones (ICRU-44).[13] Assuming an error of 10% on the extrapolation of both brain and skull attenuation coefficient, one can calculate the error made once used in the Beer-Lambert law. Considering a 1 cm thick brain slab and a 1 cm thick bone as a combination of 2×1mm of cortical bone and 8mm of spongy bone, such error will lead respectively to 3.4%/cm and 16%/cm in difference in the calculated fluorescence rate. It has also been pointed out by Verhaegen et al that the uncertainty in the tissue composition could lead to large errors in the dose deposition. Whereas the probability of the Compton effect for different tissues depends only on the electron density, the probability of photoelectric effects depends very strongly on the effective atomic number Z^{3-4} of the tissues [21]. The model used in this paper utilizes artificial mixtures that are correct for high energy photon beams but leads to large fluctuations in the retrieved fluorescence rate because the photoelectric effect is responsible for the fluorescence emission. As a consequence the retrieved fluorescence is underestimated due to an overcorrection of the number of photons when large bone thicknesses are involved. Despite difference in the retrieved fluorescence rate, using the calibration curve previously obtained the iodine

17

concentrations are in the range, between 0.1 mg/ml and 0.8 mg/ml(Table 3).

The major part of the uncertainties comes from the extrapolation procedure. In the range of energies between 28.5 keV and 80 keV the difference in photon interaction mechanism is huge for materials such as bones. Interfaces (brain/bone etc) are handled by the mean of thresholds applied depending on the pixel values. Those thresholds remain user dependant and can lead to differences in the results.

The improvement of the collimation should suppress the detection of fluorescence photons from above and below the isocenter level, and increase the accuracy of the correction based on one single CT slice at the isocenter level. One advantage of the technique is that the calculation is instantaneous, which is an added value for real *in vivo* detection.

4. Conclusion

This study is a proof of concept of detecting iodine fluorescence emission during a SSRT treatment and is a first step towards *in vivo* dosimetry in SSRT using X-ray spectroscopy. The approach in this paper helped us to point out the quantification issues in the technique. Though sensitive to the material segmentation, the technique proposed here retrieves a rough estimate of the iodine concentration in the tumor instantaneously. A range of iodine concentration ranging from 0.1 to 0.8 mg/ml has been retrieved compared to the 2 mg/ml expected. Improvements of the collimation should enhance the accuracy of the technique that can become a great added value to the SSRT project in terms of quality insurance.

5. Aknowledgement

[1] Jean-François Adam, Hélène Elleaume, Géraldine Le Duc, Stéphanie Corde, Anne-Marie Charvet, Irene Tropres, Jean-François Le Bas, and François Estève. Absolute cerebral blood volume and blood flow measurements based on synchrotron radiation quantitative computed tomography. *Journal of Cerebral Blood Flow & Metabolism*, 23(4):499–512, 2003.

[2] Peter Carmeliet and Rakesh K Jain. Angiogenesis in cancer and other diseases. *nature*, 407(6801):249, 2000.

[3] Renato Santos Mello. Radiation dose enhancement in tumors with iodine. *Medical Physics*, 10(1):75, January 1983.

[4] James Robar, Monty Martin, and Silvia Riccio. Tumor dose enhancement using modified photon beams and contrast media, April 29 2004. US Patent App. 10/621,575.

[5] Magali Edouard, David Broggio, Yolanda Prezado, François Estève, Hélène Elleaume, and Jean-François Adam. Treatment plans optimization for contrast-enhanced synchrotron stereotactic radiotherapy. *Medical physics*, 37(6Part1):2445–2456, 2010.

[6] J Holt Rose, Amos Norman, Marylou Ingram, Chuck Aoki, Tim Solberg, and Albert Mesa. First

18

radiotherapy of human metastatic brain tumors delivered by a computerized tomography scanner (ctrx). *International Journal of Radiation Oncology Biology Physics*, 45(5):1127–1132, 1999.

[7] M. Edouard, D. Broggio, Y. Prezado, F. Estève, H. Elleaume, and J. F. Adam. Treatment plans optimization for contrast-enhanced synchrotron stereotactic radiotherapy. *Medical Physics*, 37(6):2445–2456, June 2010.

[8] Layal Obeid, Pierre Deman, Alexandre Tessier, Jacques Balosso, François Estève, and Jean-François Adam. Absolute perfusion measurements and associated iodinated contrast agent time course in brain metastasis: a study for contrast-enhanced radiotherapy. *Journal of cerebral blood flow and metabolism : official journal of the International Society of Cerebral Blood Flow and Metabolism*, 34(4):638–45, April 2014.

[9] Georg-Friedemann Rust and Jörg Weigelt. X-ray fluorescent computer tomography with synchrotron radiation. *Nuclear Science, IEEE Transactions on*, 45(1):75–88, 1998.

[10] J.P. Hogan, R.A. Gonsalves, and A.S. Krieger. Fluorescent computer tomography: a model for correction of X-ray absorption. *IEEE Transactions on Nuclear Science*, 38(6):1721–1727, 1991.

[11] T. Takeda, Jin Wu Jin Wu, Thet-Thet-Lwin Thet-Thet-Lwin, N. Sunaguchi, T. Yuasa, K. Hyodo, F.a. Dilmanian, M. Minami, and T. Akatsuka. Cerebral perfusion imaging of live mice by fluorescent X-ray CT. *IEEE International Conference on Image Processing 2005*, 3(OCTOBER), 2005.

[12] Paul B. Hoffer, W. Barclay Jones, Richard B. Crawford, Robert Beck, and Alexander Gottschalk. Fluorescent Thyroid Scanning: A New Method of Imaging the Thyroid 1. *Radiology*, 90(2):342–344, February 1968.

[13] KE Goldstone. Tissue substitutes in radiation dosimetry and measurement, in: Icru report 44. international commission on radiation units and measurements, usa (1989), 1990.

[14] Lionel G Bouchet, Wesley E Bolch, David A Weber, Harold L Atkins, and John W Poston Sr. A revised dosimetric model of the adult head and brain. *The Journal of Nuclear Medicine*, 37(7):1226, 1996.

[15] MJ Berger and PSTAR ESTAR. Astar: Computer programs for calculating stopping-power and ranges for electrons. *Protons, and Helium Ions, NIST Report NISTIR-4999, Washington, DC*, 1992.

[16] Jorge E. Fernández, Viviana Scot, and Lorenzo Sabbatucci. A modeling tool for detector resolution and incomplete charge collection. *X-Ray Spectrometry*, (January):n/a–n/a, 2015.

[17] C Hall. Combined X-ray fluorescence and absorption computed tomography using a synchrotron beam. *Journal of Instrumentation*, 8(06):C06007–C06007, 2013.

[18] H Elleaume, AM Charvet, S Corde, F Esteve, and JF Le Bas. Performance of computed tomography for contrast agent concentration measurements with monochromatic x-ray beams: comparison of k-edge versus temporal subtraction. *Physics in medicine and biology*, 47(18):3369, 2002.

[19] Rene Van Grieken and Andrzej Markowicz. *Handbook of X-ray Spectrometry*. CRC Press, 2001.

[20] Wilfried Schneider, Thomas Bortfeld, and Wolfgang Schlegel. Correlation between ct numbers and tissue parameters needed for monte carlo simulations of clinical dose distributions. *Physics in medicine and biology*, 45(2):459, 2000.

[21] Frank Verhaegen, Stefan van Hoof, Patrick V Granton, and Daniela Trani. A review of treatment planning for precision image-guided photon beam pre-clinical animal radiation studies. *Zeitschrift für Medizinische Physik*, 24(4):323–334, 2014.